THESIS

NEUTRON/MUON CORRELATION FUNCTIONS TO IMPROVE NEUTRON DETECTION CAPABILITIES OUTSIDE NUCLEAR FACILITIES

Submitted by

Donald Thomas Ordinario

Department of Environmental and Radiological Health Sciences

In partial fulfillment of the requirements

For the Degree of Master of Science

Colorado State University

Fort Collins, Colorado

Summer 2016

Master's Committee:

Advisor: Alexander Brandl

Thomas Johnson
Robert Wilson

ABSTRACT

NEUTRON/MUON CORRELATION FUNCTIONS TO IMPROVE NEUTRON DETECTION CAPABILITIES OUTSIDE NUCLEAR FACILITIES

The natural neutron background rate is largely due to cosmic ray interactions in the atmosphere and the subsequent neutron emission from the interaction products. The neutron background is part of a larger cosmic radiation shower that also includes electrons, gamma rays, and muons. Since neutrons interact much differently than muons in building materials, the muon and neutron fluence rates in the natural background can be compared to the measured muon and neutron fluence rate when shielded by common building materials. The simultaneous measurement of muon and neutron fluence rates might allow for an earlier identification of man-made neutron sources, such as hidden nuclear materials. This study compares natural background neutron rates to computer simulated neutron rates shielded by common structural and building materials. The characteristic differences between neutrons and muons resulted in different attenuation properties under the same shielded conditions. Correlation functions between cosmic ray generated neutrons and muons are then used to predict neutron fluence rates in different urban environments.

TABLE OF CONTENTS

LIST OF TABLES

LIST OF FIGURES

INTRODUCTION

Cosmic Rays

Primary cosmic ray particles from the sun and from outside our solar system are incident on Earth's atmosphere. The primary cosmic ray particles constantly enter the earth's atmosphere. They consist of approximately 98% heavy nuclei and 2% electrons and positrons. Of the 98% heavy nuclei, about 87% are hydrogen, about 12% are helium, and about 1% are of heavier nuclei (Heinrich, 1999). When the primary cosmic ray particles interact with air molecules in the atmosphere, a shower of secondary cosmic ray particles is produced. These secondary particles include protons, neutrons, pions, kaons, photons, electrons and positrons (Coan, n.d.). Muons are products of the decay of pions.

The fluence rate, or the number of particles per unit area per unit time, and the energy of cosmic-ray induced particles at ground level varies with many factors. Contributing factors mainly include altitude, location in the geomagnetic field, and solar magnetic activity (Gordon, 2005). The atmospheric shielding, or atmospheric depth, is determined by the mass thickness of air per unit area above the location where cosmic radiation is measured. At sea level, earth has an atmospheric depth of approximately 1000 g/cm^2 of air which is equivalent to a depth of approximately 10 m of water. At higher altitudes, the atmospheric depth at which secondary cosmic-ray particles interact with air molecules is less therefore, higher fluence rates and energies of cosmic-ray particles are expected.

The earth's geomagnetic field deflects the charged primary cosmic particles back into space, thereby lowering the secondary cosmic ray fluence rates produced in the atmosphere. Geomagnetic fields are strongest when closer to the earth's magnetic poles and weakest when

near the equator. The minimum momentum per unit charge that a primary cosmic-ray particle can have and still reach earth's atmosphere is referred to as the geomagnetic cutoff rigidity.

Solar magnetic activity refers to the varying magnetic field from the sun that is carried outward by solar wind plasma into the solar system, thereby reducing the cosmic-ray intensity on earth. Solar magnetic activity typically follows an eleven-year cycle. Cosmic ray activity detected in the atmosphere is generally highest when solar activity is at a minimum and lowest when solar activity is at the maximum (Gordon, 2005). During maximum solar activity, more primary cosmic ray particles are deflected outside of the atmosphere and back into space, therefore fewer interactions occur in the atmosphere resulting in a lower cosmic ray fluence rate on the ground.

Cosmic-ray Induced Muon Theory

One type of secondary cosmic particles are pions. Pions have a maximum vertical fluence rate at an altitude of about 15 km above sea level and spontaneously decay to a muon plus a neutrino or antineutrino. Muons generally lose about 2 GeV of energy due to ionization prior to reaching the ground. The energy and angular distribution of the muons at ground level is a function of the production spectrum, energy loss in the atmosphere, and decay. The energy spectrum of muons at a 0^{o} angular distribution is almost flat below 1 GeV, increases gradually to reflect a fluence rate plateau in the 10–100 GeV range, and slowly falls off at higher energies because higher energy pions, where bremsstrahlung and ionization rates are equal, tend to interact in the atmosphere before they decay (Review of Particle Physics, 2014).

Muons have a mean-life of 2.197 μs, mass of 105.658 MeV/c^2, and are produced by the decay of pions at approximately 15 km above sea level (Olive, 2014). Using the muon as the

reference frame, a muon with a momentum of 10 GeV/c would only travel 660 m, however due to the time dilation effect of special relativity, the muon is able to reach sea level and can be detected on the ground. Using the equation for relativistic momentum, and solving for velocity (Turner, 2007):

$$p = \gamma m u$$

$$\gamma = \frac{p}{mu}$$

$$\gamma = \frac{1}{\sqrt{\left(1 - \frac{u^2}{c^2}\right)}}$$

$$u = \frac{cp}{\sqrt{m^2c^2 + p^2}} = \frac{10\,\frac{\mathrm{GeV}}{c} \times c}{\sqrt{0.105658\,\frac{\mathrm{GeV}}{c^2} \times c^2 + \left(10\,\frac{\mathrm{GeV}}{c}\right)^2}} \sim 1c$$

Where, p = muon momentum (GeV/c)
m = mass = 0.105658 GeV/c^2
u = muon velocity
c = speed of light = 3×10^8 m/s
γ = Lorentz transformation factor

At a muon momentum of 10 GeV/c, the velocity of the muon is equal to the speed of light. To determine the length of travel of the muon in reference to an observer on the ground, the Lorentz transformation factor must be determined and multiplied by the proper length traveled, or simply the product of velocity and time.

$$\gamma = \frac{p}{mu} = \frac{10\,\frac{\mathrm{GeV}}{c}}{0.105658\,\frac{\mathrm{Gev}}{c^2} \times 1c} = 94.7$$

$$L = u \times \Delta t$$

$$L = \left(3 \times 10^8\,\frac{\mathrm{m}}{\mathrm{s}}\right) \times (2.197 \times 10^{-6}\mathrm{s}) = 660\ \mathrm{m}$$

$$L' = \gamma L = 94.7 \times 660 \text{ m} = 62{,}500 \text{ m}$$

Where, Δt = mean life of a muon = 2.197 μs
L = proper length traveled in rest frame
L' = length traveled relative to an observer on earth

Because of the theory of relativity, the 10 GeV/c muon can actually travel up to 62,500 m, and therefore reach sea level and beyond before decaying. Muons reaching sea level with excess momentum are therefore stopped deep in the earth's crust and lithosphere (Review of Particle Physics, 2014).

Cosmic-ray Induced Neutron Theory and Simulation

Secondary cosmic ray particles also include neutrons. Neutrons are generated when the primary cosmic ray particles collide with atoms in the atmosphere. The primary cosmic ray particles lose energy due to ionization with the air atoms, resulting in continuous slowing down of the primary cosmic ray particle. With each collision, the primary cosmic ray particle loses about 50% of its energy, resulting in the production of secondary cosmic ray particles, including neutrons (Heinrich, 1999).

The cosmic-ray induced neutrons measured at ground level are plotted on an energy spectrum where the fluence is on the ordinate and the neutron energy (E) is on a logarithmic scale on the abscissa. The neutron energy distribution has three distinct peaks: a high-energy peak around 100 MeV and extending to about 10 GeV, a nuclear evaporation peak around 1 MeV, and a thermal peak at 10^{-7} MeV. The thermal peak is where neutrons have slowed due to scattering to the point where they are in thermal equilibrium with the surrounding atoms (Gordon, 2004). An example of a typical neutron energy spectrum showing all three broad peaks is illustrated in Figure 1.

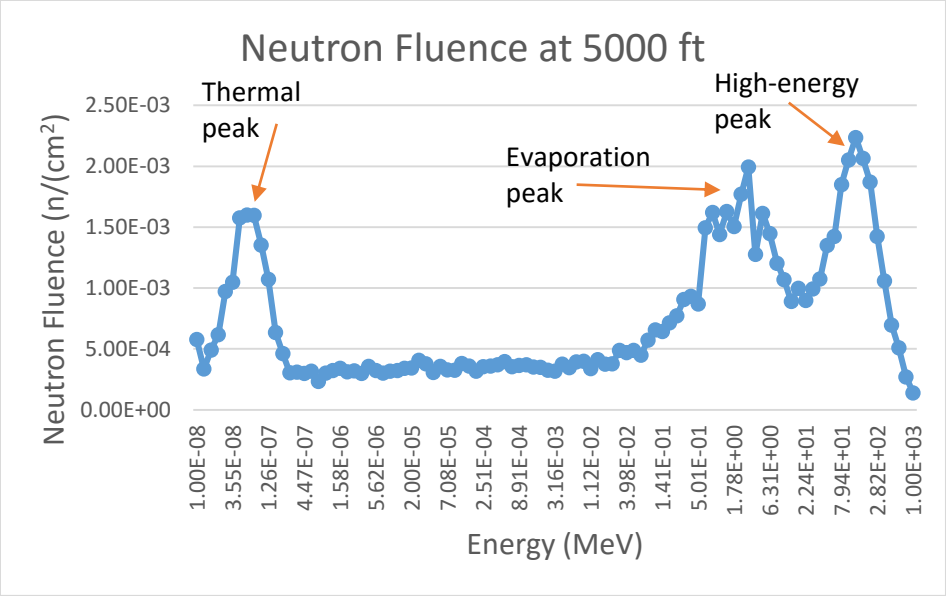

Figure 1: Neutron energy distribution with three distinct energy peaks.

Computer simulation of background cosmic-ray neutrons on the ground is possible by using the MCNP6 background source capability (Fensin, 2013). In 2012, the capability to simulate the solar and galactic cosmic ray source spectrum was added to MCNP6 where the user provides a location using latitude and longitude coordinates, and a date. The location coordinates chosen by the user provide the cosmic ray spectrum with the correct altitude and magnetic rigidity. The date entered adjusts the energy spectrum with the correct intensity from solar modulation effects (Fensin, 2013). Background cosmic ray neutrons and photons were placed in a data file, titled background.dat, based on one generic background source spectrum from New York with scaling constants for neutrons on a 10°×10° longitude and latitude grid around the world (Fensin, 2013).

Neutron and Muon Characteristics

The production of cosmic-ray neutrons and muons is different and so are other characteristics. Table 1 summarizes some of the differences between neutrons and muons.

Table 1. Characteristic differences of cosmic-ray muons and neutrons.

Particle	Symbol/Charge	Antiparticle	Mass	Energy	Mean life
Neutrons	n/Neutral	$\bar{n}$/Neutral	939.6 MeV/c^2	10^{-8} MeV to 10^3 MeV	881.5 s
Muons	μ^-/Negative	μ^+/Positive	105.66 MeV/c^2	0.2 GeV to 404 GeV	2.197 µs

The differences noted in Table 1 highlight some of the factors that affect how cosmic-ray neutrons and muons in this study will interact with matter.

Man-made Neutron Sources

Compact, portable neutron sources such as ^{252}Cf can be fabricated and used in laboratory settings, for verifying proper operation of instruments, or for irradiating samples. Man-made neutron sources can also be produced by combining alpha emitters with elements such as beryllium, lithium, fluorine, or other elements where (α,n) reactions are possible (Ensslin, n.d.). Two common (α,n) neutron sources are ^{241}AmBe and ^{240}AmLi. In addition to fabricated neutron sources used for laboratory work, nuclear weapons containing highly enriched uranium or plutonium are also sources of man-made neutron radiation. Because of this, detection of man-made neutron sources is an important part of national security. Nuclear weapons contain fissile material including either weapons-grade uranium (WgU) or weapons-grade plutonium (WgPu).

Neutrons are produced from the fissile material primarily though spontaneous fission. Spontaneous fission occurs when the strong, short-range nuclear forces attempt to hold a nucleus together against the electrostatic repulsion of the protons. For the heaviest elements such as uranium and plutonium, the repulsive forces of the protons are so strong that the nucleus is barely held together. There is a small but finite probability that nucleus will split, or spontaneously fission, and form two fission fragments, and within 10^{-13} seconds, emit prompt neutrons and gamma rays (Ensslin, n.d.). Isotopes of plutonium, in particular ^{240}Pu, undergo spontaneous fission at a higher rate than isotopes of uranium, so the neutron signature coming from a plutonium weapon would generally be higher than that of a uranium weapon. In addition to spontaneous fission, neutrons are produced in nuclear weapons from the (α,n) reactions where light elements such as oxygen, which is also present in nuclear weapons, absorb an alpha particle and emit a neutron (Fetter, 1990). An example of a typical (α,n) in nuclear fuels is:

$$\alpha + {}^{18}\mathrm{O} \rightarrow {}^{21}\mathrm{Ne} + \mathrm{n}$$

The average energy of an alpha particle that is emitted from uranium is 4.7 MeV. For plutonium, the average alpha energy is 5.2 MeV (Ensslin, n.d.). For both elements, the emitted alpha energy is high enough to overcome the Coulomb barrier of the target nucleus and have excess energy to emit a neutron. The total neutron yield from both spontaneous fission and (α,n) reaction is 1.60 neutrons per second per kg of WgU and 56,000 neutrons per second per kg of WgPu.

Muon Detection

Muons can be detected using two separate scintillation detectors placed at a distance from each other and attached to a photomultiplier tube. As muons interact with the scintillating

material, creating photons of light, the photomultiplier tube collects the light and generates an electrical signal. The electrical signal can then be sent to an amplifier and registered using a standard nuclear instrumentation counting setup. Two separate scintillators are used to measure the coincidence rate. Time of flight hodoscopes are used along with the scintillators to provide velocity and energy loss calculations (Haino, 2004). Since other charged particles such as electrons, positrons, and alpha particles have relatively short track lengths in comparison to muons, signals from these charged particles would be registered in only one of the two scintillation counters. When the coincidence signal is registered from both the upper and lower time of flight counter, the system will count the signal as muon particle. The surface area of the scintillators, and the distance separating the scintillators is used to determine the muon counts per unit area and also the solid angle subtended (Ankney, n.d.).

Neutron Detection

Active neutron detection generally involves a nuclear reaction which results in the prompt energetic release of charged particles such as protons or alpha particles. ^{3}He gas filled proportional counters have commonly been used in the detection of cosmic ray induced neutrons. ^{3}He is used as a detection medium for neutrons though the following reaction:

$$^{3}_{2}\mathrm{He} + ^{1}_{0}\mathrm{n} \rightarrow ^{3}_{1}\mathrm{H} + ^{1}_{1}\mathrm{p}$$

The resulting proton can then be counted due to the ionization it produces in the gas filled chamber. Various thicknesses of high-density polyethylene spheres surround the detector in order to detect neutrons of varying energies. The larger the moderator, the higher the energy of incident neutrons that the detector counts with good detection efficiency (Gordon, 2005). For detection of higher energy neutrons >30 MeV, other materials can be added on the outside of the

polyethylene sphere such as lead and steel. High-energy neutrons interacting with lead or iron nuclei causes hadronic showers with secondary neutrons that are easily detected. With increasing neutron energy, the instrument would indicate a rising response (Gordon, 2005). For detection of a wide spectrum of neutron energies, multiple detectors need to be used.

Current neutron detection technology provides the capability to detect low levels of neutron activity with very high efficiency. In urban environments, or where a man-made neutron source may be shielded and hidden within a structural building, neutron detectors by themselves would not be able to distinguish between neutrons that are cosmic-ray induced and man-made neutrons that are shielded within the building. False positive detection events, where radiation is detected from a source other than the special nuclear material (SNM) of interest and classified as coming from SNM, would be more common if the threshold for detection was unknown. Cosmic ray generated neutrons detected within a building could be incorrectly classified as a man-made neutron source. Conversely, a false negative detection event could occur where low activity neutrons detected from SNM within a building would be incorrectly classified as cosmic ray background radiation.

In order to increase the detection efficiency of man-made neutron sources in urban environments, a comparison can be made between cosmic ray muons and cosmic ray neutrons under an unknown thickness of common building materials. Because of the different properties between muons and neutrons, the thickness required to shield muons is much higher than that required to shield neutrons. The difference allows the development of correlation functions to predict a cosmic neutron fluence rate based on the fluence rate of muons that are detected within a building.

Since altitude plays a major role in the energy distribution of muons and neutrons, correlation functions were developed at three different altitudes. Sea level, 2000 feet (610 m), and 5000 feet (1524 m) were chosen as the altitudes where correlation functions were determined. Additionally, attenuation of the muons and neutrons differ depending on the building material used, and the thickness of the material shielding the detector. Three different common building materials were analyzed in the development of the neutron/muon correlation functions. Thicknesses ranging from 0 to 500 cm were used for concrete, brick, and steel constructed buildings.

Monte Carlo based radiation transport modeling was used to determine the attenuation of neutrons and muons and to develop the correlation functions. Monte Carlo n-Particle 6 (MCNP6), developed by Los Alamos National Laboratory, was used for the neutron and muon particle transport model. MCNP6 is widely used within the nuclear engineering, health physics, and medical physics industries and has been benchmarked and validated for many different applications.

MATERIALS AND METHODS

Muon energy distribution

Muon energy distributions used in the MCNP input files were determined from published literature of different muon studies. The sea level muon energy distribution was input based on measurements using muon detectors in Tsukuba, Japan (Haino, 2004). The fluence rate of positively charged muons was added to the fluence rates of negatively charged muons for each energy bin of muons. The sum in each energy bin was divided by the total muon fluence rate to determine the distribution of muons in each energy bin. The distribution of muons in each energy bin is the probability that a cosmic-ray muon will have an energy within a particular bin. Muon momenta range from 0.576 GeV/c to 404 GeV/c.

The same method of calculating the distribution of muon energies was repeated for muons at an altitude of 1181 feet and 4167 feet. The muon fluence rate at an altitude of 1181 feet was measured using the CAPRICE muon detector at Lynn Lake, Manitoba, Canada in 1994 (Kremer, 1999). The same CAPRICE muon detector was used at Fort Sumner, New Mexico in 1997 (Kremer, 1999). Of all available muon measurement data at altitude, the CAPRICE muon detector studies conducted in 1994 and 1997 were chosen because the altitudes where the data were collected were close to the altitudes of interest of 2000 ft and 5000 ft.

Table 2 summarizes the CAPRICE94 and CAPRICE97 data for altitudes of 1181 ft (360 m) and 4167 ft (1270 m), respectively. The total combined muon fluence rate difference between the two altitudes was 57.9 muons/(cm^2 s sr). The fluence rate at 4167 ft compared to the fluence rate at 1181 ft, using a similar detection method, increased by 16.9% with an altitude increase of 2,987 ft. Using this ratio, an altitude of 5000 ft as compared to 4167 ft would

increase the total fluence rate by only 0.473%, and an altitude of 2000 ft compared to 1181 ft would increase the total fluence rate by only 0.465%. Based on the data in Figure 2 and Table 2, an estimation of the muon energy distribution at 5000 feet would be expected to be similar to the measured energy distribution at 4167 feet. The same argument holds true for estimating the muon energy distribution at 2000 ft compared to the measured muon energy distribution at 1181 ft.

Table 2. Combined muon fluence rates at altitudes of 1181 ft and 4167 ft using CAPRICE94 and CAPRICE97 data (Kremer, 1999).

			Altitude		
			1180 ft	4167 ft	
Momentum Range (GeV/c)		Mean Momentum (GeV/c)	Combined Muon Fluence Rate (Muons/cm^2 s sr)		Difference (Muons/cm^2 s sr)
0.2	0.3	0.25	2.50E+01	2.27E+01	-2.30E+00
0.3	0.4	0.35	3.04E+01	3.22E+01	1.80E+00
0.4	0.55	0.47	3.16E+01	3.82E+01	6.60E+00
0.55	0.7	0.62	3.01E+01	3.98E+01	9.70E+00
0.7	0.85	0.78	2.89E+01	3.80E+01	9.10E+00
0.85	1	0.92	2.69E+01	3.56E+01	8.70E+00
1	1.2	1.1	2.40E+01	3.25E+01	8.50E+00
1.2	1.4	1.3	2.21E+01	2.83E+01	6.20E+00
1.4	1.6	1.5	1.89E+01	2.53E+01	6.40E+00
1.6	2.1	1.84	1.64E+01	1.62E+01	-2.00E-01
2.1	2.94	2.49	1.18E+01	1.27E+01	9.00E-01
2.94	4.12	3.49	7.50E+00	8.66E+00	1.16E+00
4.12	5.5	4.78	4.51E+00	5.26E+00	7.50E-01
5.5	7	6.21	2.86E+00	3.15E+00	2.90E-01
7	10	8.37	1.59E+00	1.80E+00	2.10E-01
10	15.5	12.42	6.98E-01	7.34E-01	3.60E-02
15.5	23	18.85	2.46E-01	2.70E-01	2.40E-02
23	31.1	26.68	1.09E-01	1.09E-01	0.00E+00
31.1	43.6	36.69	4.70E-02	4.83E-02	1.30E-03
43.6	61.1	51.47	1.70E-02	1.79E-02	9.00E-04
61.1	85.6	72.08	6.60E-03	7.40E-03	8.00E-04
85.6	120	100.96	2.60E-03	2.60E-03	0.00E+00
		Total	**2.84E+02**	**3.42E+02**	**5.79E+01**

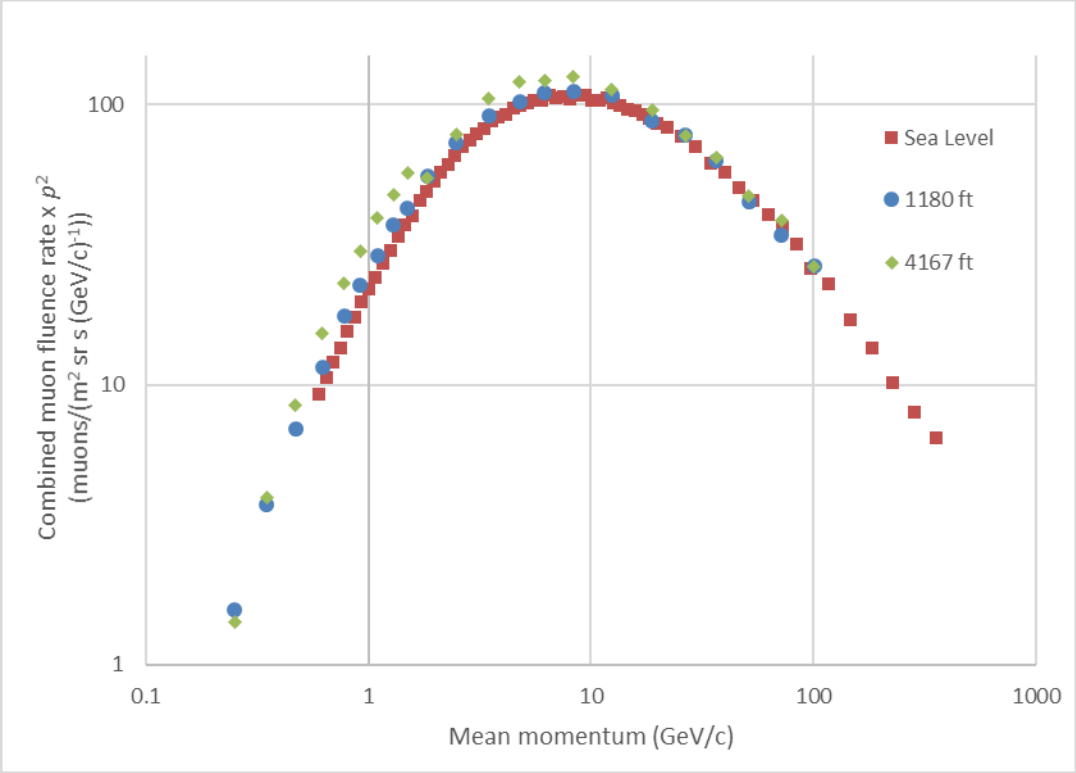

Figure 2: Combined muon fluence rate distribution (Haino, 2004)(Kremer, 1999).

Neutron energy distribution

Neutron fluence and energy distributions were simulated using the MCNP6 background source option. Neutron energy distributions are listed in the background.dat file within MCNP6 for latitude and longitudinal locations globally. Locations within the continental United States were chosen based on their altitudes. The location chosen for sea level was at 40N 70W, near New York City, NY. For 2000 ft altitude, the location coordinates chosen were 40N 80W, which is located in Fredrickstown, PA, 40 miles south of Pittsburgh, PA. At an altitude of 5000 ft, location coordinates were 40N 110W in Duchesne, UT, 100 miles east of Salt Lake City, UT.

For each of the locations, a uniform isotropic neutron source was created within a 1000 m^3 cube with an energy distribution specific to the altitude and location. A sphere with a diameter of 40 cm was created in the center of the cube and an MCNP F4 cell volume tally of the

neutron fluence spectrum within the sphere was counted. In order to reduce uncertainties, each MCNP input file was run with 10 million starting particles. The neutron output was tallied in logarithmically scaled energy bins ranging from 1×10^{-8} MeV to 1000 MeV. Similar to the muons, the fluence rate within each energy bin was divided by the total fluence rate to determine the energy distribution for the neutrons. Consequently, the neutron energy distribution was input as the energies and probabilities in the MCNP input file source card. Figure 3 illustrates the MCNP6 simulated neutron fluence for each of the energy bins at sea level, 2000 ft, and 5000 ft.

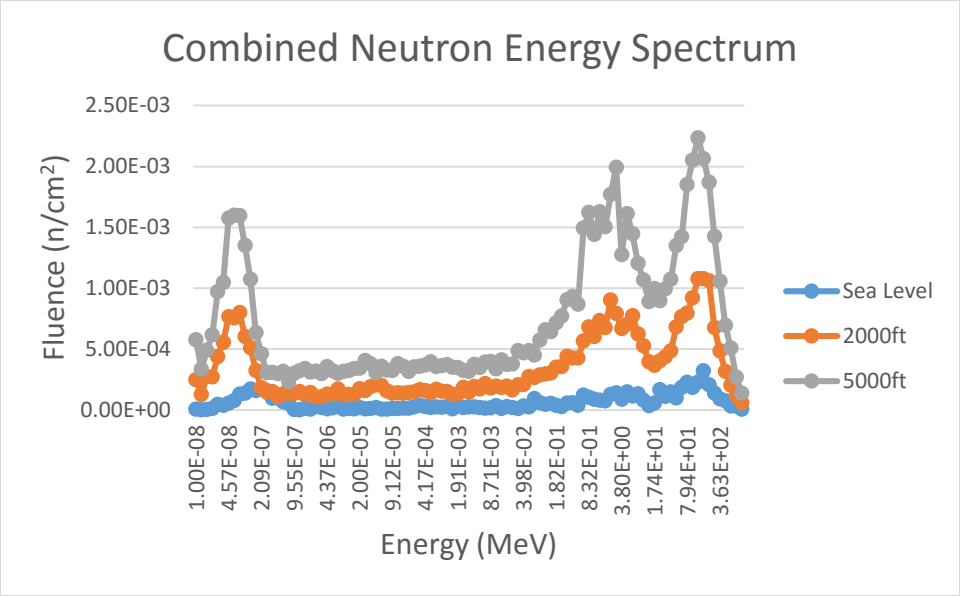

Figure 3. MCNP6 generated neutron energy spectrum at sea level, 2000 ft, and 5000 ft.

Total neutron fluence rates were also determined from the background.dat file within MCNP6. Neutron fluence rates are displayed in Table 3.

Table 3. Background cosmic-ray neutron fluence rates. (MCNP6 background.dat)

Location	Altitude (ft)	Neutron Fluence Rate (n/cm^2 s)
40N 70W	0	1.59215×10^{-2}
40N 80W	2000	3.55629×10^{-2}
40N 110W	5000	7.62025×10^{-2}

MCNP input file

For both muons and neutrons, the MCNP geometry was identical. A 1000 m^3 cube was created with a plane source placed at the very top surface of the cube. The source was evenly distributed throughout the plane and was directed down towards the bottom of the cube. The source particles and their energy distributions were entered based on the particle and altitude.

A detector volume was created as a 20 cm × 20 cm × 1 cm parallelepiped located 1 meter above the bottom of the cube. Both the volume of the cube and the detector volume were filled with air. An F4 cell volume tally was counted within the detector volume with a total of 10 million starting particles. An F4 tally counts the number of particles that pass through a volume. Because the MCNP cell tally output is reported in units of number of particles per cm^2, and the source was a unidirectional 1×10^6 cm^2 plane, a tally multiplier of 1×10^6 was applied to calculate the number of neutrons per square centimeter. If unshielded, all of the particles above the detector volume would be counted. Since the plane source is unidirectional and evenly distributed, the source would average out to 1 particle per cm^2. As shielding is applied, the number of particles per cm^2 decreases to less than one and translates to the fraction of particles that transmit through the shielding.

When adding the building material, another parallelepiped was placed between the source and the detector. The parallelepiped extended the entire length and width of the cube, and varied in thickness from 25 cm to 500 cm. Atomic weights for concrete, steel, and brick were added to the material cards, and densities were added to the cell cards within the MCNP input files. Particle importance was set to 1 for the particle identified in the source card, either neutrons or muons. The MCNP geometry used in all simulations is illustrated in Figure 4.

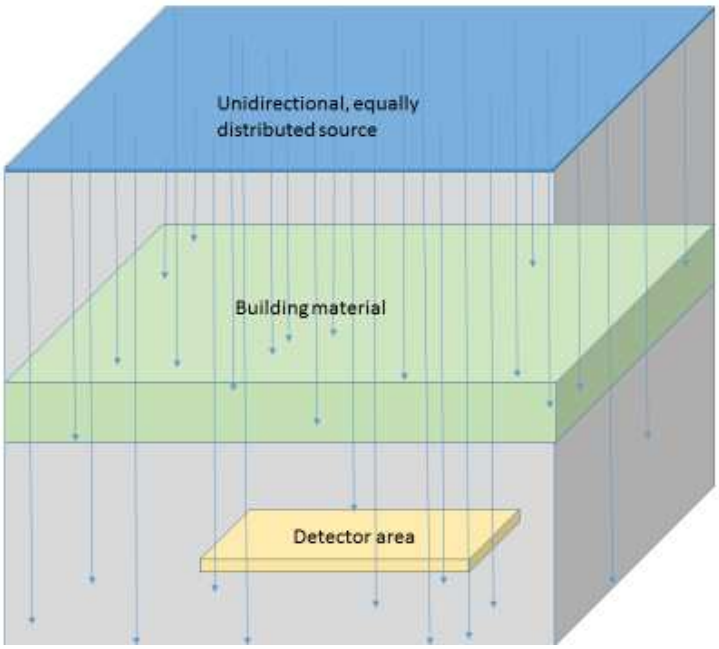

Figure 4. MCNP geometry for simulation of cosmic-ray particle attenuation through various thicknesses of building material.

Input files for neutrons and muons were run with 10 million starting particles for all three altitudes and with all three common building materials. For concrete and brick, twenty simulations were performed for each altitude at thicknesses of 25 cm to 500 cm in 25 cm increments. For steel, ten simulations were performed in increments of 50 cm from 50 cm to 500 cm.

MCNP output file

MCNP F4 volume cell tally output with the tally multiplier of 1×10^{6} provides an estimate of the fraction of particles that transmitted through the attenuator material. The fractions were plotted for both neutrons and muons. At each altitude, three plots for both neutrons and muons were created for visualization of the effect of attenuating thickness on the fluence rate of the incident cosmic-ray particle. The three plots are representative of the building material;

concrete, brick, and steel. The fraction of neutrons that transmitted through the material thickness over the fraction of muons that transmitted the same thickness was calculated to provide the correlation function.

RESULTS

Sea Level

Using source cards with the cosmic-ray neutron and muon energies and energy probabilities, the percentage of the unshielded fluence rate is plotted as a function of building material thickness. Table 4 displays the MCNP6 output fluence rate penetration factors for muons and neutrons through all three building materials. Figure 5 shows the neutron and muon attenuation curve for thicknesses of concrete from 0 cm to 500 cm. Figure 6 provides a plot of the neutron and muon attenuation for brick, and Figure 7 displays the data for steel. Fraction transmitted data points greater than 1.0 are within the MCNP output statistical uncertainty.

Table 4. MCNP6 output summary for sea level muon and neutron transmission factors through various thicknesses of concrete, brick, and steel.

	Concrete		Brick		Steel	
Thickness (cm)	Muon	Neutron	Muon	Neutron	Muon	Neutron
0	1.00947E+00	9.98296E-01	1.00947E+00	9.98296E-01	1.00947E+00	9.98296E-01
25	1.00860E+00	5.00601E-01	9.96219E-01	6.70821E-01		
50	1.00431E+00	2.40068E-01	1.01141E+00	4.52934E-01	9.52326E-01	2.15815E-01
75	1.00332E+00	9.77141E-02	9.89991E-01	3.21502E-01		
100	1.01662E+00	3.56190E-02	1.00314E+00	2.21475E-01	4.82391E-01	4.57843E-02
125	1.00457E+00	1.31222E-02	9.93136E-01	1.27840E-01		
150	9.32776E-01	4.07250E-03	9.97092E-01	8.06885E-02	2.83643E-01	1.49784E-02
175	8.08205E-01	1.55991E-03	1.00781E+00	5.38788E-02		
200	7.31928E-01	1.71450E-04	9.15790E-01	2.56971E-02	1.86215E-01	1.23494E-03
225	6.62702E-01	4.96699E-04	8.14579E-01	1.58967E-02		
250	5.86889E-01	1.84058E-04	7.38289E-01	4.43831E-03	1.18065E-01	4.21916E-04
275	5.22605E-01	0.00000E+00	6.88711E-01	2.81350E-03		
300	4.76525E-01	0.00000E+00	6.25640E-01	1.74440E-03	8.47274E-02	2.38090E-04
325	4.38739E-01	0.00000E+00	5.73928E-01	3.92799E-04		
350	4.07817E-01	0.00000E+00	5.29471E-01	8.91549E-04	6.07084E-02	0.00000E+00
375	3.68450E-01	0.00000E+00	4.91382E-01	0.00000E+00		
400	3.29201E-01	0.00000E+00	4.51752E-01	0.00000E+00	4.93485E-02	0.00000E+00
425	3.15072E-01	0.00000E+00	4.33652E-01	0.00000E+00		
450	2.98276E-01	0.00000E+00	4.06487E-01	0.00000E+00	3.66656E-02	0.00000E+00
475	2.78712E-01	0.00000E+00	3.80753E-01	0.00000E+00		
500	2.48661E-01	0.00000E+00	3.43979E-01	0.00000E+00	3.19665E-02	0.00000E+00

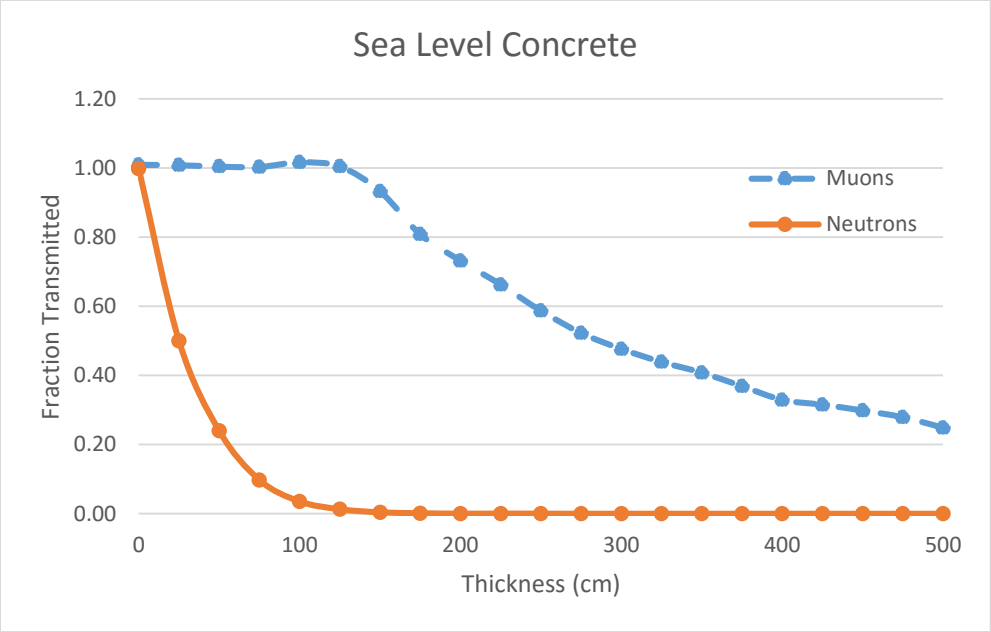

Figure 5. Sea level cosmic-ray muon and neutron attenuation as a function of varying thicknesses of concrete.

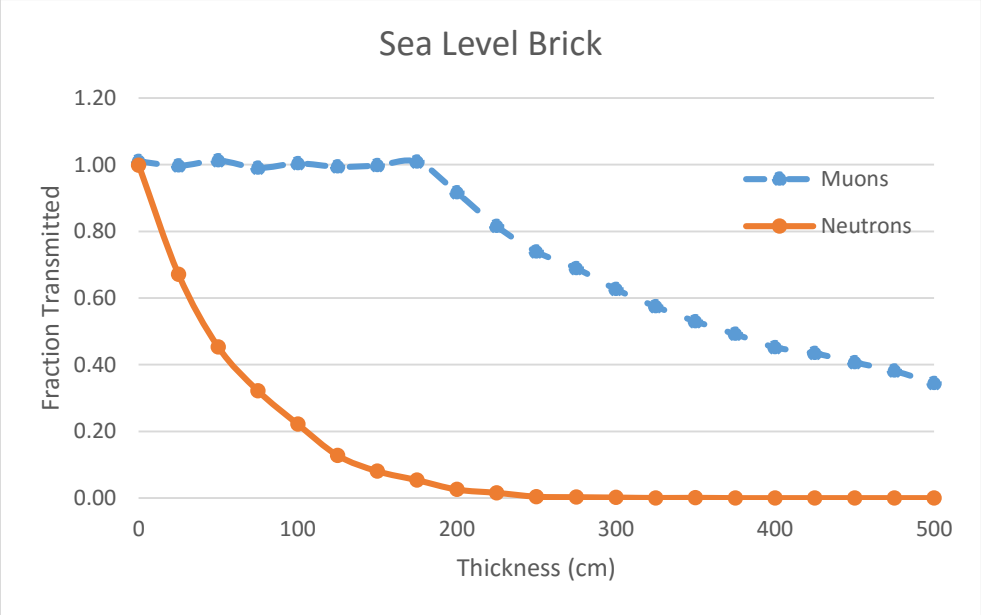

Figure 6. Sea level cosmic-ray muon and neutron attenuation as a function of varying thicknesses of brick.

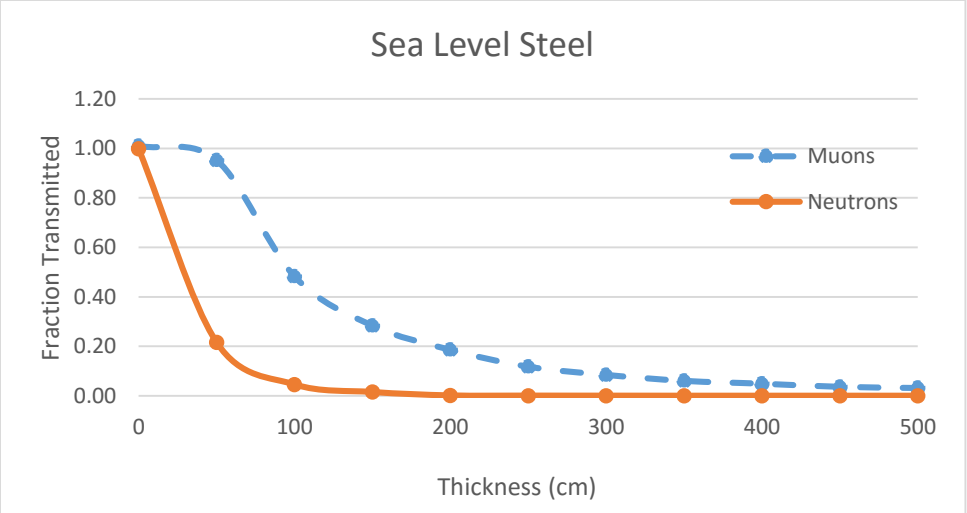

Figure 7. Sea level cosmic-ray muon and neutron attenuation as a function of varying thicknesses of steel.

Correlation functions for cosmic-ray neutrons and muons are listed in Table 5.

Table 5. Neutron/muon correlation functions at sea level.

SEA LEVEL Neutron/Muon Correlation Functions			
Thickness (cm)	Concrete	Brick	Steel
0	0.988931	0.988931	0.988931
25	0.496333	0.673367	
50	0.239038	0.447824	0.226619
75	0.097391	0.324752	
100	0.035037	0.220782	0.094911
125	0.013063	0.128724	
150	0.004366	0.080924	0.052807
175	0.00193	0.053461	
200	0.000234	0.02806	0.006632
225	0.00075	0.019515	
250	0.000314	0.006012	0.003574
275	0	0.004085	
300	0	0.002788	0.00281
325	0	0.000684	
350	0	0.001684	0
375	0	0	
400	0	0	0
425	0	0	
450	0	0	0
475	0	0	
500	0	0	0

2000 ft

At 2000 ft, the MCNP source card is modified to include the energies and probability distributions for neutrons and muons at an altitude of approximately 2000 ft. The tally count in the MCNP output file is plotted to illustrate the fraction of incoming cosmic ray neutrons and muons that transmit through the building material and are counted by an F4 tally in the detector area. Table 6 displays the MCNP6 output fluence rate penetration factors for muons and neutrons through all three building materials. Figure 8 provides a plot of the 2000 ft data using concrete as the attenuator. Figure 9 uses brick, and Figure 10 uses steel. Fraction transmitted data points greater than 1.0 are within the MCNP output statistical uncertainty.

Table 6. MCNP6 output summary for muon and neutron transmission factors through various thicknesses of concrete, brick, and steel at an altitude of 2000 ft.

	Concrete		Brick		Steel	
Thickness (cm)	Muon	Neutron	Muon	Neutron	Muon	Neutron
0	9.98199E-01	9.88040E-01	9.98199E-01	9.88040E-01	9.98199E-01	9.88040E-01
25	1.01238E+00	4.43908E-01	9.97960E-01	6.28332E-01		
50	1.00253E+00	1.96085E-01	1.00018E+00	4.08612E-01	9.17662E-01	1.97306E-01
75	1.01098E+00	7.82236E-02	9.88348E-01	3.10034E-01		
100	1.02843E+00	2.58558E-02	1.00124E+00	2.06965E-01	3.98425E-01	4.67006E-02
125	1.00088E+00	1.09028E-02	9.87418E-01	1.09372E-01		
150	9.10470E-01	3.64876E-03	1.00148E+00	7.20999E-02	1.81126E-01	1.48700E-02
175	7.99953E-01	6.78660E-04	9.90069E-01	3.89138E-02		
200	6.95026E-01	7.36859E-04	8.81497E-01	2.24046E-02	1.11303E-01	9.27065E-04
225	5.92990E-01	5.08643E-04	7.94242E-01	1.21611E-02		
250	5.39381E-01	1.84051E-04	7.25574E-01	4.86363E-03	7.80793E-02	6.39742E-04
275	4.67055E-01	0.00000E+00	6.44802E-01	2.23216E-03		
300	4.01711E-01	0.00000E+00	5.56094E-01	9.78480E-04	5.46351E-02	2.38090E-04
325	3.43731E-01	0.00000E+00	5.08116E-01	7.32543E-04		
350	2.90721E-01	0.00000E+00	4.74190E-01	7.27283E-04	4.18286E-02	0.00000E+00
375	2.44000E-01	0.00000E+00	4.10924E-01	0.00000E+00		
400	2.17998E-01	0.00000E+00	3.75158E-01	1.46040E-04	2.82092E-02	0.00000E+00
425	2.00078E-01	0.00000E+00	3.21945E-01	0.00000E+00		
450	1.75673E-01	0.00000E+00	2.73429E-01	0.00000E+00	2.63231E-02	0.00000E+00
475	1.64300E-01	0.00000E+00	2.37943E-01	0.00000E+00		
500	1.47714E-01	0.00000E+00	2.06696E-01	0.00000E+00	1.43877E-02	0.00000E+00

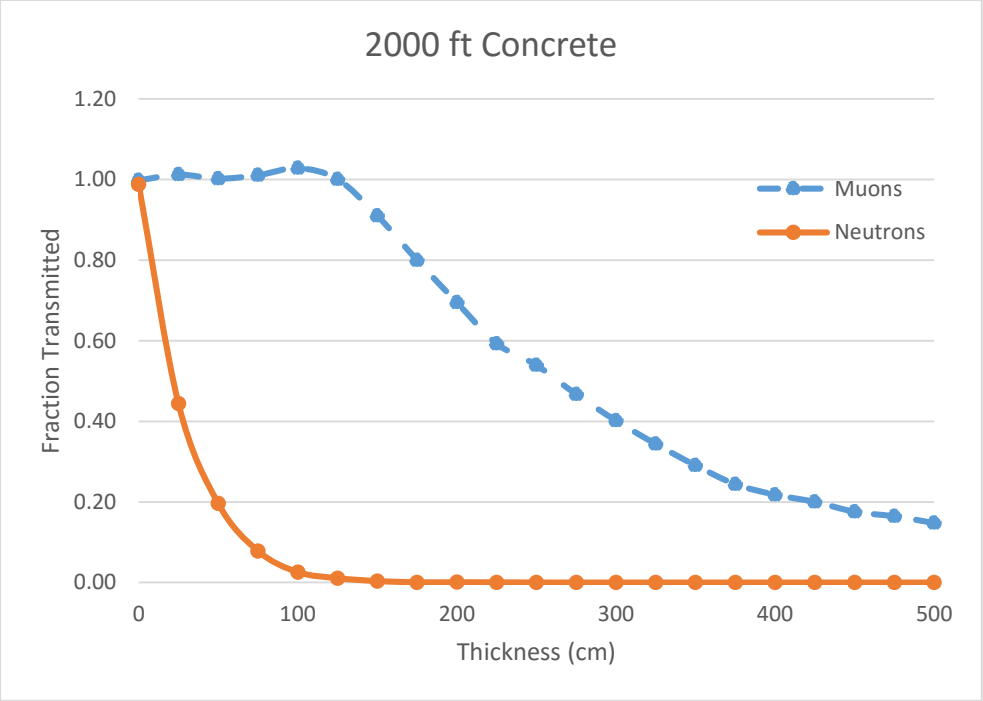

Figure 8. Cosmic-ray muon and neutron attenuation at an altitude of 2000 ft as a function of varying thicknesses of concrete.

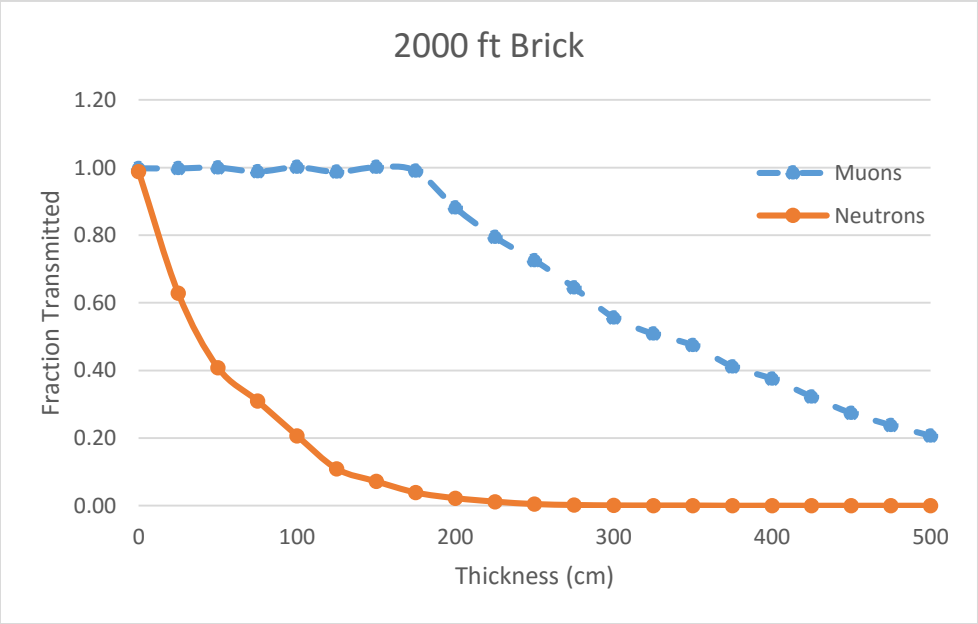

Figure 9. Cosmic-ray muon and neutron attenuation at an altitude of 2000 ft as a function of varying thicknesses of brick.

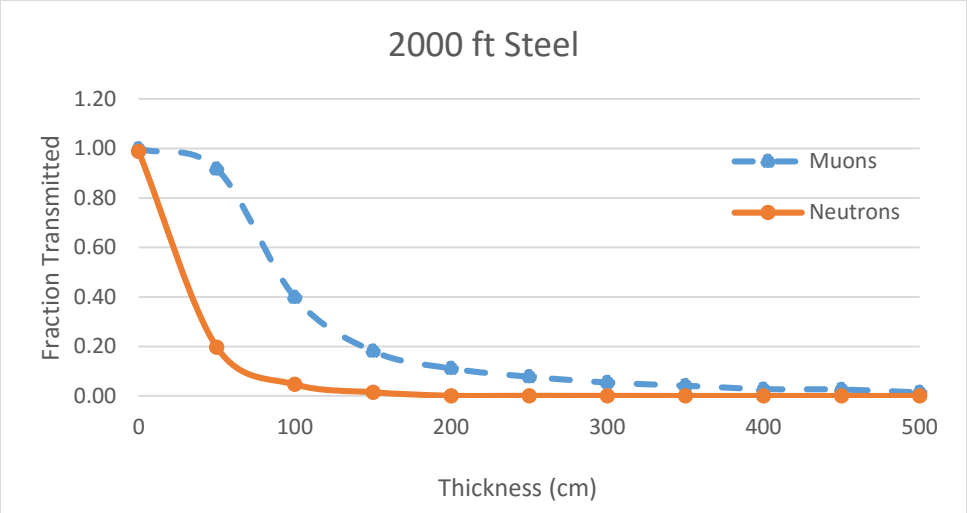

Figure 10. Cosmic-ray muon and neutron attenuation at an altitude of 2000 ft as a function of varying thicknesses of steel.

A summary of neutron to muon correlation functions at 2000 ft is listed in Table 7.

Table 7. Neutron/muon correlation functions at 2000 ft.

2000 ft Neutron/Muon Correlation Functions			
Thickness (cm)	Concrete	Brick	Steel
0	0.989823	0.989823	0.989823
25	0.43848	0.629616	
50	0.19559	0.408538	0.215009
75	0.077374	0.313689	
100	0.025141	0.206709	0.117213
125	0.010893	0.110766	
150	0.004008	0.071993	0.082098
175	0.000848	0.039304	
200	0.00106	0.025417	0.008329
225	0.000858	0.015312	
250	0.000341	0.006703	0.008193
275	0	0.003462	
300	0	0.00176	0.004358
325	0	0.001442	
350	0	0.001534	0
375	0	0	
400	0	0.000389	0
425	0	0	
450	0	0	0
475	0	0	
500	0	0	0.00000

5000 ft

At an altitude of 5000 ft, the energies and probability distributions of the cosmic-ray neutrons and muons differ from an altitude of 2000 ft and from sea level. The MCNP source card probability distribution is changed. Since the method of muon measurement between 2000 ft and 5000 ft was the same, the source energies on each source card are identical. The output tally data are plotted again as a function of building material thicknesses. Table 8 displays the MCNP6 output fluence rate penetration factors for muons and neutrons through all three building materials. Figure 11 displays the cosmic-ray muon and neutron attenuation curves at 5000 ft using concrete as the attenuator. Figure 12 uses brick as the attenuator, and Figure 13 uses steel. Fraction transmitted data points greater than 1.0 are within the MCNP output statistical uncertainty.

Table 8. MCNP6 output summary for sea level muon and neutron transmission factors through various thicknesses of concrete, brick, and steel at an altitude of 5000 ft.

	Concrete		Brick		Steel	
Thickness (cm)	Muon	Neutron	Muon	Neutron	Muon	Neutron
0	9.95303E-01	9.89438E-01	9.98199E-01	9.88040E-01	9.95303E-01	9.89438E-01
25	1.01336E+00	4.35501E-01	9.97960E-01	6.28332E-01		
50	1.00671E+00	1.91573E-01	1.00018E+00	4.08612E-01	5.36704E-01	1.82639E-01
75	1.01199E+00	7.16411E-02	9.88348E-01	3.10034E-01		
100	1.02369E+00	2.34820E-02	1.00124E+00	2.06965E-01	1.86189E-01	3.73838E-02
125	1.00185E+00	1.15067E-02	9.87418E-01	1.09372E-01		
150	9.01926E-01	3.11753E-03	1.00148E+00	7.20999E-02	7.95660E-02	1.18020E-02
175	7.90854E-01	1.00348E-03	9.90069E-01	3.89138E-02		
200	6.84124E-01	2.09716E-04	8.81497E-01	2.24046E-02	4.36446E-02	2.35491E-04
225	5.76843E-01	7.29809E-04	7.94242E-01	1.21611E-02		
250	5.02325E-01	1.84053E-04	7.25574E-01	4.86363E-03	2.83972E-02	4.21916E-04
275	4.42156E-01	0.00000E+00	6.44802E-01	2.23216E-03		
300	3.65289E-01	0.00000E+00	5.56094E-01	9.78480E-04	1.79981E-02	2.38090E-04
325	3.26174E-01	0.00000E+00	5.08116E-01	7.32543E-04		
350	2.62265E-01	0.00000E+00	4.74190E-01	7.27283E-04	1.14235E-02	0.00000E+00
375	2.12737E-01	0.00000E+00	4.10924E-01	0.00000E+00		
400	1.82971E-01	0.00000E+00	3.75158E-01	1.46040E-04	8.32808E-03	0.00000E+00
425	1.62882E-01	0.00000E+00	3.21945E-01	0.00000E+00		
450	1.54798E-01	0.00000E+00	2.73429E-01	0.00000E+00	5.57994E-03	0.00000E+00
475	1.46358E-01	0.00000E+00	2.37943E-01	0.00000E+00		
500	1.31667E-01	0.00000E+00	2.06696E-01	0.00000E+00	2.77112E-03	0.00000E+00

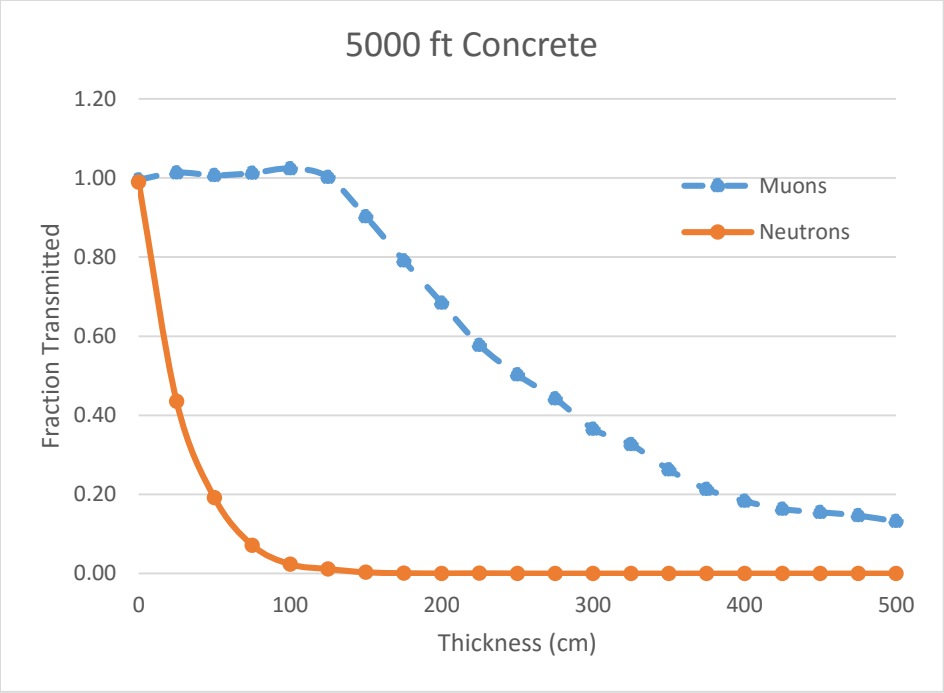

Figure 11. Cosmic-ray muon and neutron attenuation at an altitude of 5000 ft as a function of varying thicknesses of concrete.

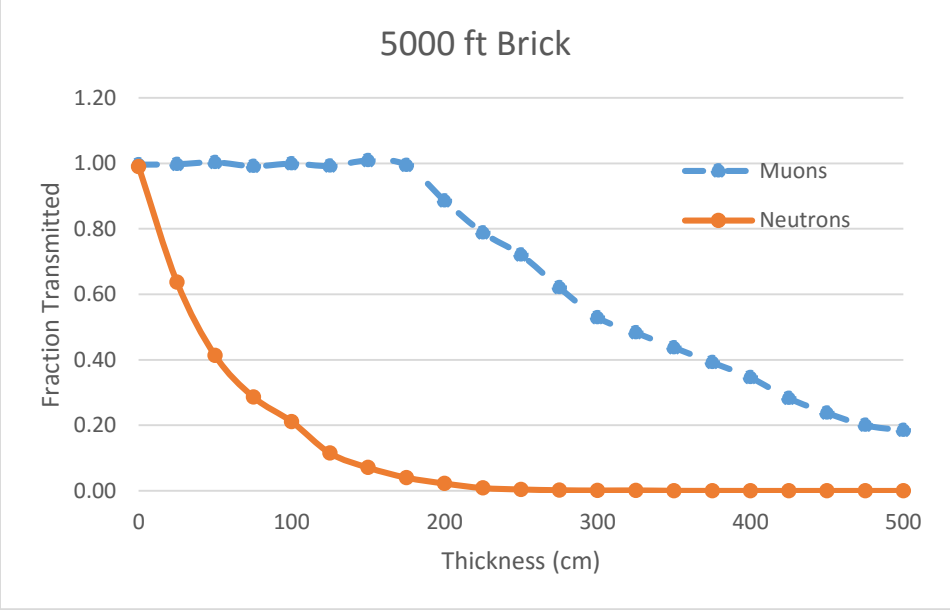

Figure 12. Cosmic-ray muon and neutron attenuation at an altitude of 5000 ft as a function of varying thicknesses of brick.

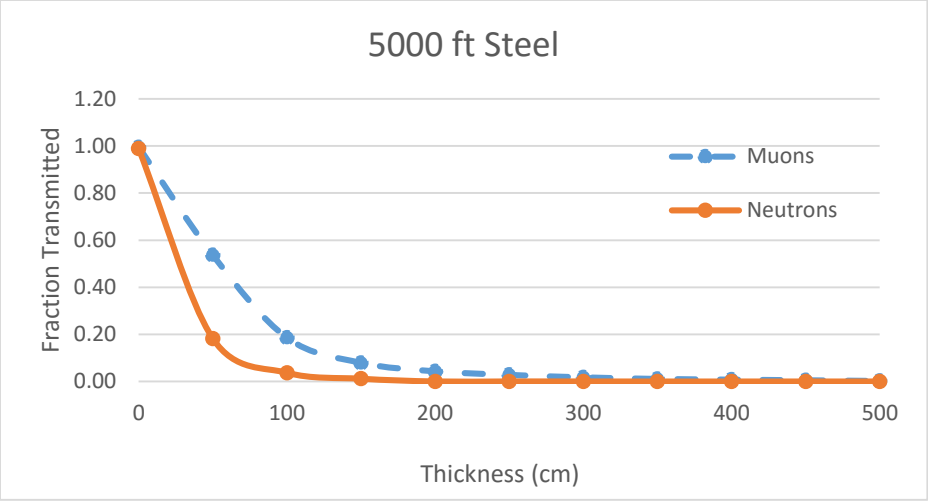

Figure 13. Cosmic-ray muon and neutron attenuation at an altitude of 5000 ft as a function of varying thicknesses of steel.

Table 9 displays the neutron/muon correlation functions at 5000 ft.

Table 9. Neutron/muon correlation functions at 5000 ft.

5000 ft Neutron/Muon Correlation Functions			
Thickness (cm)	Concrete	Brick	Steel
0	0.994107	0.99411	0.994107
25	0.429759	0.63967	
50	0.190296	0.41201	0.340297
75	0.070792	0.28931	
100	0.022939	0.21175	0.200784
125	0.011485	0.11642	
150	0.003457	0.07053	0.14833
175	0.001269	0.04078	
200	0.000307	0.02554	0.005396
225	0.001265	0.01117	
250	0.000366	0.00621	0.014858
275	0	0.00346	
300	0	0.00245	0.013229
325	0	0.00328	
350	0	0.00082	0
375	0	0.00035	
400	0	0.00000	0
425	0	0.00000	
450	0	0.00000	0
475	0	0.00000	
500	0	0.00000	0

DISCUSSION

Using the raw data for muon energies at all three altitudes initially provided results that were not consistent with expectations. After careful review of the data and comparisons with the input, the difference in expectations is determined to be due to the different energy ranges recorded from sea level and the energy ranges at approximately 2000 ft and 5000 ft. Since the raw data were from two separate studies, using two different measurement methods, the muon energy and distribution information used to simulate how the muons interact with the attenuators did not result in a comparable study. Using the same energy range for all three altitudes was determined to alleviate the issue and provide more meaningful results. The momentum range common to all three studies ranged from 600 MeV/c to 101 GeV/c. In order to provide the same range for the mean momentum for all three altitudes, the highest six data points at sea level and the lowest three data points at 1180 ft and 4167 ft were removed. Figure 14 shows the combined muon fluence rate as a function of the mean momentum.

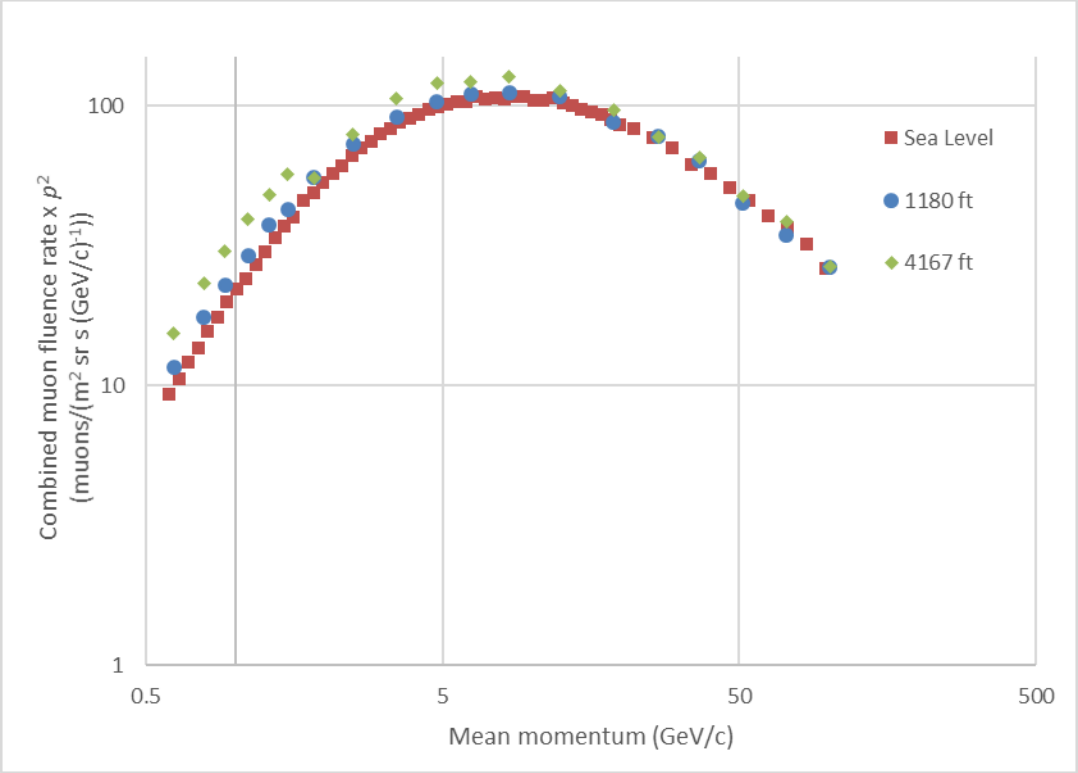

Figure 14: Combined muon fluence rate distribution as a function of the chosen mean momentum range (Haino, 2004)(Kremer, 1999).

Once a similar mean momentum range was used for muons, the comparison of attenuation properties between neutrons and muons could be made. For all altitudes and shielding materials used, the fraction of cosmic-ray neutrons that are detected beneath the material follows an exponentially decreasing trend as the thickness of building material increases. The rate at which the exponential decrease occurs is dependent on the material used.

Steel and concrete have a similar ability to attenuate neutrons and have a near equal rate of absorption with increasing material thickness. Although steel has a higher density at 8 g/cm^3 than concrete, which has a density of 2.3 g/cm^3, the composition of concrete has a higher concentration of hydrogen, which is much more effective at moderating neutrons than steel, which contains 99% iron by mass fraction. The rate of absorption in concrete and steel are

higher than that of brick, meaning cosmic-ray neutrons are stopped at lower thicknesses of concrete and steel compared to brick. At around 200 cm of concrete and steel, the fraction of neutrons which reached the detector was less than 0.01% of the original neutron fluence rate. Around 300 cm of brick is required to reduce the neutron fluence rate to the same amount. Brick has the lowest density of the three materials at 1.80 g/cm^3, and also does not contain any hydrogen. These two factors contribute to the lower neutron attenuation characteristics.

Essentially all of the muons had sufficient energy to transmit through up to 125 cm of concrete and up to 175 cm of brick. After the initial thickness of concrete and brick, the fraction of muons penetrating the material decreased slowly following an exponential curve. For steel, thicknesses as low as 50 cm at sea level are able to stop approximately 5% of the cosmic-ray muons from entering the detector area. At greater thicknesses, the fraction of muons transmitting through follows a steep exponential decrease. The muon curve for steel is much different from that for concrete and brick due to the different chemical composition and higher density.

In order to utilize the correlation between the cosmic-ray muon and neutron fluence rate in an environment where cosmic radiation is shielded by an unknown thickness of a material, an operator must first determine what the unshielded fluence rate values are for both muons and neutrons. With no shielding, the number of particles reaching the detector area would be 100%. With the baseline fluence rate values, the correlation of muons to neutrons can be used when detecting the cosmic-ray particles inside of a building.

The operator must take muon measurements inside the building and calculate the percent of the baseline unshielded muons measured. With the fraction of muons still being detected within the building, the effective thickness of building material that is shielding the detector can be determined by looking at the appropriate curve or table for the main construction material

used. The material used in the construction of the building may use multiple materials such as steel reinforced concrete, however the curve or table used in estimating the effective thickness would be the main material used in the construction of the building.

When the effective thickness of shielding material is determined, the graph or table can be used to determine what the expected percentage of detected cosmic-ray neutrons would be at the same location where the muon measurements were taken. If the measured neutron count is higher than the expected value, then a determination can be made that the presence of another neutron source may be hidden nearby. The threshold at which additional investigation is required should be where the operator's measurement, at a 95% confidence level, is above the expected neutron count rate. A discrepancy between measured and expected neutron fluence rates could be used to prompt additional and more thorough searches within the building.

The neutron fluence rate decision threshold where an operator would investigate further for hidden neutron sources is calculated using the following equation:

$$\text{Decision Threshold } = \mu + 1.645\sigma$$

Where, σ = standard deviation = $\sqrt{\mu/time}$
μ = background neutron fluence rate

Neutron fluence rate decision thresholds, at altitudes of sea level, 2000 ft and 5000 ft are calculated in Table 10.

Table 10. Neutron fluence rate decision thresholds.

		Decision Thresholds (n/cm^2)		
Altitude (ft)	Neutron Fluence Rate (n/cm^2 s)	1 second count	1 minute count	10 minute count
0	1.592E-02	2.235E-02	4.272E-02	2.440E-02
2000	3.556E-02	3.458E-02	7.561E-02	4.823E-02
5000	7.620E-02	5.303E-02	1.348E-01	9.474E-02

For a 1 m^2 neutron detector at sea level with 100% efficiency, an operator would expect to see a background neutron fluence of 159 counts per second (cps). The decision threshold at which further investigation would be required is a measured neutron fluence at or above 2235 cps for a 1 second background measurement. At an altitude of 2000 ft, the expected background neutron fluence would be 355 cps and the decision threshold would be 3458 cps, using the same 100%, 1 m^2 neutron detector. At 5000 ft, the background neutron fluence would be 762 cps, with a decision threshold of 5303 cps. If one minute measurements were to be used instead of one second measurements, the decision thresholds would reduce to 427 cps, 756 cps, and 1348 cps for altitudes of sea level, 2000 ft, and 5000 ft, respectively. Furthermore, if 10 minute counts were performed, the decision threshold would be further reduced to 244 cps, 482 cps, and 947 cps, for altitudes of sea level, 2000 ft, and 5000 ft, respectively. Essentially, the sensitivity of neutron source detection increases as the amount of time that the operator is able to take a neutron measurement increases.

For shielding thicknesses of up to 125 cm for concrete and 175 cm for brick, where the cosmic-ray muons have sufficient energy to completely transmit through the material, determining the effective thickness of the building material would require additional analysis using a separate method. For the neutrons however, a large percentage of cosmic-ray neutrons are absorbed by the concrete or brick material. The expected neutron fluence rate within a building where the measured shielded muon fluence rate is equal to the unshielded baseline value could be anywhere from the expected neutron fluence rate at a minimum thickness of up to 125 cm for concrete and 175 cm for brick. When the effective thickness is determined to be less than 125 cm concrete or 175 cm brick, the use of the muon to neutron relationship will not be as accurate; however, it can still be used to determine the presence of an external neutron source.

For example, if the measured muon fluence rate inside of a one story concrete or brick structure is the same as the unshielded baseline, and the measured neutron fluence rate is also equal to the unshielded baseline, then the operator can use the correlation table or graph to determine that the measured neutron fluence rate is higher than expected. The minimum thickness of a concrete roof flat slab is approximately 10 cm (Concrete Roof Systems, n.d.), where approximately 20% of cosmic-ray neutrons would be absorbed. Even though the effective thickness of shielding material is known only to be less than 125 cm concrete or 175 cm brick, a range of the expected neutron fluence rate can be determined from the correlation graph or table.

Between 200 cm and 350 cm for all materials, the neutron fluence was shielded to <0.01% of the original unshielded fluence. Even though essentially all of the neutrons were absorbed, the neutron to muon correlation relationship can still be used. If the measured muon fluence rate resulted in an effective thickness of any building material to be high enough that all neutrons are absorbed, then any neutron counts detected could be from a man-made source.

CONCLUSION

Characteristics such as mass, energy, charge, momentum, and fluence rates affect how an incident particle interacts with matter. The characteristic differences between cosmic-ray induced muons and neutrons leads to the ability to compare attenuation capabilities in varying thicknesses of common building materials. Based on radiation transport modeling using MCNP 6, the differences in attenuation of cosmic-ray muons and neutrons were compared in concrete, brick, and steel. The characteristics of cosmic-ray particles are also heavily influenced by the altitude and location where measurements are taken. Computer modeling of cosmic-ray muons and neutrons provided simulations at altitudes of sea level, 2000 ft, and 5000 ft.

Since the cosmic-ray muons and neutrons proved to have different attenuation curves with increasing thickness of building material, the measured muon fluence rate within a structure could be used to determine an effective thickness of material shielding the particles, and therefore the expected neutron fluence rate at the effective thickness. This correlation function could prove to be useful for radiological monitoring crews in early detection of man-made neutron sources such as nuclear weapons.

The method used in this study to determine the fluence rates of cosmic-ray neutrons and muons would not be the same method used by operators in the field. The data used in this study were analyzed to determine the feasibility of using neutron to muon correlation functions for increased detection sensitivity of man-made neutron sources in urban environments. In order to create specific neutron to muon correlation tables and graphs for the operator, the energy range and sensitivity of the specific instruments must be taken into account and computer modeling performed for those specific instruments.

In order to prove the effectiveness of the neutron/muon correlation function method of neutron radiation detection, field experiments would need to be performed. The computer simulated natural background neutron and muon fluence rates would need to be verified, along with the attenuation curves with varying thicknesses of common building material. Verification could either be conducted by stacking slabs of building material over the detectors and taking measurements, or by comparing field data from homeland security radiological monitoring teams. Unfortunately, no such data were available during conduct of this study, so computer modeling was the only method analyzed.

Once data specific to neutron and muon detectors in use are analyzed and verified, finalized neutron to muon correlation charts and tables could be provided to radiological monitoring teams taking measurements in urban areas. The raw data used in the MCNP6 models in this experiment showed a clear difference in the attenuation properties between muons and neutrons. Even with adjusting the energy ranges of both muons and neutrons, the attenuation differences would still be large enough to be used as an early neutron source detection method. The method is simple and could potentially be used regularly in the search for clandestine nuclear materials.

REFERENCES

1. Heinrich, W., & Schraube, H. (1999). Physics of Cosmic Radiation Fields. *Radiation Protection Dosimetry, 86*(4), 253-258.

2. Haino, S. et al. (2004). Measurements of primary and atmospheric cosmic-ray spectra with the BESS-TeV spectrometer. *Physics Letters B, 594*, 35-46.

3. Coan, T. E., Ye, J. *Muon Physics*.

4. Review of Particle Physics. Particle Data Group. (2014). *Chinese Physics C, 38*(9), 378-385.

5. Olive, K. A., et al. Particle Data Group. (2014). Chin. Phys. C38, 09001.

6. Turner, J. E. (2007). *Atoms, radiation, and radiation protection*. New York: Pergamon Press.

7. Gordon, M. S. (2004). Measurement of the Flux and Energy Spectrum of Cosmic-Ray Induced Neutrons on the Ground. *IEEE Transactions on Nuclear Science,51*(6), 3427-3434.

8. M.L. Fensin & G.W. McKinney, "How to use the MCNP6 Background Source Capability", 2013 ANS Winter Meeting, Washington, LA-UR-13-23344 (2013).

9. Concrete Roof Systems. (n.d.). Retrieved May 24, 2016, from http://www.concreteconstruction.net/Images/Concrete Roof Systems -- Part II_ Cast-in-Place Construction_tcm45-348521.pdf

10. Fetter, S., et al. (1990). Detecting Nuclear Warheads. *Science & Global Security, 1*, 225-302.

11. Ensslin, N. (n.d.). The Origin of Neutron Radiation.

12. Ankney, A., et al. Muon Fluence Measurements for Homeland Security Applications. *Pacific Northwest National Laboratory, PNNL-19632*.

13. Kremer, J., et al. (1999). Measurements of Ground-Level Muons at Two Geomagnetic Locations. *Physical Review Letters, 83*(21), 4241-4244.

14. Knoll, G. F. (2010). *Radiation Detection and Measurement* (4th ed.). New York: Wiley.

APPENDIX A

MCNP6 input file to determine cosmic-ray neutron energy distribution at sea level

```
c -----Uniform isotropic neutron source in a cube----------
c -------cell cards--------------------
c 1 2 -0.00012048 -1 2 imp:|=1
c 2 2 -0.00012048 -2 imp:|=1
1 0 -1 2 imp:n=1
2 0 -2 imp:n=1
3 0 1 imp:n=0

c -------surface cards----------------------
1 rpp -500 500 -500 500 -500 500
2 so 20

c material cards
c ------------------
c Concrete standard p=2.3 g cm-3
c ----------------------
c m1 1001 0.1170 8016 0.6082 14000 0.2748
c --------------------------
c Air p=1.2048x10 -4 g cm-3
c --------------------------
c m2 7014 -0.7553 8016 -0.2318 18000 -0.01282 6012 -0.000125
c -------------------------------
c Source Definition
c -------------------
mode n
SDEF PAR=bn x=d1 y=d2 z= d3 wgt=1.621621e6 $SA/F=6*1000*1000/3.7
    LOC=40 -75 0 $ New York
si1 -500 500
sp1 0 1
si2 -500 500
sp2 0 1
si3 -500 500
sp3 0 1
fc2 Tally neutron flux on sphere surface
f2:n 2
fc4 Tally neutron flux in small sphere
f4:n 2
fc14 Neutron flux spectrum in sphere
f14:n 2
e14 1e-8 99log 1e3
```

```
nps 100000000
print
```

APPENDIX B

MCNP6 input file to determine cosmic-ray neutron energy distribution at 2000 ft

```
c -----Uniform isotropic neutron source in a cube----------
c -------cell cards--------------------
c 1 2 -0.00012048 -1 2 imp:|=1
c 2 2 -0.00012048 -2 imp:|=1
1 0 -1 2 imp:n=1
2 0 -2 imp:n=1
3 0 1 imp:n=0

c -------surface cards----------------------
1 rpp -500 500 -500 500 -500 500
2 so 20

c material cards
c ------------------
c Concrete standard p=2.3 g cm-3
c ----------------------
c m1 1001 0.1170 8016 0.6082 14000 0.2748
c --------------------------
c Air p=1.2048x10 -4 g cm-3
c --------------------------
c m2 7014 -0.7553 8016 -0.2318 18000 -0.01282 6012 -0.000125
c --------------------------------
c Source Definition
c -------------------
mode n
SDEF PAR=bn x=d1 y=d2 z= d3 wgt=1.621621e6 $SA/F=6*1000*1000/3.7
    LOC=40 -80 0.7 $ Fredrickstown, PA, near Pittsburgh
si1 -500 500
sp1 0 1
si2 -500 500
sp2 0 1
si3 -500 500
sp3 0 1
fc2 Tally neutron flux on sphere surface
f2:n 2
fc4 Tally neutron flux in small sphere
f4:n 2
fc14 Neutron flux spectrum in sphere
f14:n 2
e14 1e-8 99log 1e3
```

```
nps 100000000
print
```

APPENDIX C

MCNP6 input file to determine cosmic-ray neutron energy distribution at 5000 ft

```
c -----Uniform isotropic neutron source in a cube----------
c -------cell cards--------------------
c 1 2 -0.00012048 -1 2 imp:|=1
c 2 2 -0.00012048 -2 imp:|=1
1 0 -1 2 imp:n=1
2 0 -2 imp:n=1
3 0 1 imp:n=0

c -------surface cards----------------------
1 rpp -500 500 -500 500 -500 500
2 so 20

c material cards
c ------------------
c Concrete standard p=2.3 g cm-3
c ----------------------
c m1 1001 0.1170 8016 0.6082 14000 0.2748
c --------------------------
c Air p=1.2048x10 -4 g cm-3
c --------------------------
c m2 7014 -0.7553 8016 -0.2318 18000 -0.01282 6012 -0.000125
c --------------------------------
c Source Definition
c -------------------
mode n
SDEF PAR=bn x=d1 y=d2 z= d3 wgt=1.621621e6 $SA/F=6*1000*1000/3.7
    LOC=40 -110 1.6 $ Duchesne, UT, near Salt Lake City
si1 -500 500
sp1 0 1
si2 -500 500
sp2 0 1
si3 -500 500
sp3 0 1
fc2 Tally neutron flux on sphere surface
f2:n 2
fc4 Tally neutron flux in small sphere
f4:n 2
fc14 Neutron flux spectrum in sphere
f14:n 2
e14 1e-8 99log 1e3
```

```
nps 100000000
print
```

APPENDIX D

MCNP6 input file to determine attenuation of cosmic-ray muons at sea level

```
c -----MUON BOX----------
c -------cell cards--------------------
1 2 -0.00012048 -1 2 3 imp:|=1
2 2 -0.00012048 -2 imp:|=1
3 0 1 imp:|=0
4 4 -1.8 -3 imp:|=1

c -------surface cards----------------------
1 rpp -500 500 -500 500 -500 500
2 rpp -10 10 -10 10 -400 -399
3 rpp -499.9 499.9 -499.9 499.9 -300 -200

c material cards
c ------------------
c Concrete standard p=2.3 g cm-3
c ----------------------
c m1 1001 0.1170 8016 0.6082 14000 0.2748
c --------------------------
c Air p=1.2048x10 -4 g cm-3
c --------------------------
m2 7014 -0.7553 8016 -0.2318 18000 -0.01282 6012 -0.000125
c -------------------------------
c Steel SAE 1020 p=8.0 g cm-3
c --------------------
c m3 6000 -0.002 26000 -0.991
c ---------------------
c Brick, common silica p=1.80 g cm-3
c ----------------------------
m4 8016 0.663432 13027 0.003747 14000 0.323225 20000 0.007063 26000 0.002534
c ----------------------
c Source Definition
c -------------------
mode |
PHYS:| 5e6
SDEF PAR=| x=d1 y=d2 z= 500 vec 0 0 -1 dir 1 erg=d3
c SDEF PAR=| x=d1 y=d2 z= 500 vec 0 0 -1 dir 1 erg=1000
si1 h -500 500
sp1 d 0 1
si2 h -500 500
sp2 d 0 1
```

```
si3 576 621 669 720 776 836 901 970 1040 1130 1210 &
   1310 1410 1520 1630 1760 1900 2040 2200 2370 2550 2750 2960 3190 &
   3440 3710 3990 4300 4630 4990 5380 5790 6240 6730 7250 7810 8410 &
   9060 9760 10500 11300 12200 13200 14200 15300 16400 17700 19100 &
   20600 23900 27700 32100 37300 43300 50200 58300 67700 78500 91100 &
   106000
sp3 0 5.487E-02 5.402E-02 5.317E-02 5.127E-02 5.063E-02 4.894E-02 4.809E-02 &
   4.576E-02 4.364E-02 4.194E-02 4.025E-02 3.879E-02 3.684E-02 3.442E-02 &
   3.349E-02 3.087E-02 2.900E-02 2.699E-02 2.487E-02 2.315E-02 2.133E-02 &
   1.930E-02 1.760E-02 1.585E-02 1.451E-02 1.286E-02 1.142E-02 1.027E-02 &
   9.067E-03 7.986E-03 7.054E-03 6.080E-03 5.444E-03 4.597E-03 4.004E-03 &
   3.398E-03 2.998E-03 2.587E-03 2.163E-03 1.854E-03 1.614E-03 1.339E-03 &
   1.140E-03 9.448E-04 8.071E-04 6.694E-04 5.593E-04 4.618E-04 3.586E-04 &
   2.485E-04 1.695E-04 1.099E-04 7.542E-05 4.978E-05 3.320E-05 2.173E-05 &
   1.460E-05 9.491E-06 5.762E-06
f14:| 2
fc14 Muon flux through RPP
FM14 1e6
nps 10000000
```

APPENDIX E

MCNP6 input file to determine attenuation of cosmic-ray muons at 2000 ft

```
c -----MUON BOX----------
c -------cell cards--------------------
1 2 -0.00012048 -1 2 3 imp:|=1
2 2 -0.00012048 -2 imp:|=1
3 0 1 imp:|=0
4 1 -2.3 -3 imp:|=1

c -------surface cards----------------------
1 rpp -500 500 -500 500 -500 500
2 rpp -10 10 -10 10 -400 -399
3 rpp -499.9 499.9 -499.9 499.9 -300 -200

c material cards
c ------------------
c Concrete standard p=2.3 g cm-3
c ----------------------
m1 1001 0.1170 8016 0.6082 14000 0.2748
c --------------------------
c Air p=1.2048x10 -4 g cm-3
c --------------------------
m2 7014 -0.7553 8016 -0.2318 18000 -0.01282 6012 -0.000125
c --------------------------------
c Steel SAE 1020 p=8.0 g cm-3
c --------------------
c m3 6000 -0.002 26000 -0.991
c --------------------
c Brick, common silica p=1.80 g cm-3
c ----------------------------
c m4 8016 0.663432 13027 0.003747 14000 0.323225 20000 0.007063 26000 0.002534
c ---------------------
c Source Definition --- J. Kremer et al./Physical Review Letters Vol 83 no 21 (1999) Table 1
c ------------------- Location: Lynn Lake, Manitoba, Canada 1180 ft (360 m)
mode |
PHYS:| 5e6
SDEF PAR=| x=d1 y=d2 z= 500 vec 0 0 -1 dir 1 erg=d3
si1 h -500 500
sp1 d 0 1
si2 h -500 500
sp2 d 0 1
si3 550 700 850 1000 1200 1400 1600 2100 2940 4120 5500 &
```

```
   7000 10000 15500 23000 31100 43600 61100 85600 120000
sp3 0 1.530E-01 1.469E-01 1.368E-01 1.220E-01 1.124E-01 &
   9.609E-02 8.338E-02 5.999E-02 3.813E-02 2.293E-02 &
   1.454E-02 8.084E-03 3.549E-03 1.251E-03 5.542E-04 &
   2.390E-04 8.643E-05 3.356E-05 1.322E-05
f14:| 2
fc14 Muon flux through RPP
FM14 1e6
nps 10000000
```

APPENDIX F

MCNP6 input file to determine attenuation of cosmic-ray muons at 5000 ft

```
c -----MUON BOX----------
c -------cell cards--------------------
1 2 -0.00012048 -1 2 3 imp:|=1
2 2 -0.00012048 -2 imp:|=1
3 0 1 imp:|=0
4 3 -8 -3 imp:|=1

c -------surface cards----------------------
1 rpp -500 500 -500 500 -500 500
2 rpp -10 10 -10 10 -400 -399
3 rpp -499.9 499.9 -499.9 499.9 -300 -200

c material cards
c ------------------
c Concrete standard p=2.3 g cm-3
c ----------------------
c m1 1001 0.1170 8016 0.6082 14000 0.2748
c --------------------------
c Air p=1.2048x10 -4 g cm-3
c --------------------------
m2 7014 -0.7553 8016 -0.2318 18000 -0.01282 6012 -0.000125
c --------------------------------
c Steel SAE 1020 p=8.0 g cm-3
c --------------------
m3 6000 -0.002 26000 -0.991
c ---------------------
c Brick, common silica p=1.80 g cm-3
c ----------------------------
c m4 8016 0.663432 13027 0.003747 14000 0.323225 20000 0.007063 26000 0.002534
c ----------------------
c Source Definition --- J. Kremer et al./Physical Review Letters Vol 83 no 21 (1999) Table 1
c ------------------- Location: Fort Sumner, NM 4167 ft (1270 m)
mode |
PHYS:| 5e6
SDEF PAR=| x=d1 y=d2 z= 500 vec 0 0 -1 dir 1 erg=d3
si1 h -500 500
sp1 d 0 1
si2 h -500 500
sp2 d 0 1
si3 0 200 300 400 550 700 850 1000 1200 1400 1600 2100 2940 4120 5500 &
```

```
   7000 10000 15500 23000 31100 43600 61100 85600
sp3 0 0.0665 0.0943 0.112 0.117 0.111 0.104 0.0952 0.0829 0.0741 &
   0.0474 0.0372 0.0254 0.0154 0.00922 0.00527 0.00215 7.9e-4 3.19e-4 &
   1.41e-4 5.24e-5 2.17e-5 7.61e-6
c f2:| 2
c f12:| 2
c fc12 Muon flux through surface
c e12 1e-8 99log 1e3
c f4:| 2
f14:| 2
fc14 Muon flux through RPP
FM14 1e6
nps 10000000
```

APPENDIX G

MCNP6 input file to determine attenuation of cosmic-ray neutrons at sea level

```
c --------NEUTRON BOX ------------------
c -------cell cards--------------------
1 2 -0.00012048 -1 2 3 imp:n=1
2 2 -0.00012048 -2 imp:n=1
3 0 1 imp:n=0
4 1 -2.3 -3 imp:n=1

c -------surface cards----------------------
1 rpp -500 500 -500 500 -500 500
2 rpp -10 10 -10 10 -400 -399
3 rpp -499.9 499.9 -499.9 499.9 -300 -200

c material cards
c ------------------
c Concrete standard p=2.3 g cm-3
c ----------------------
m1 1001 0.1170 8016 0.6082 14000 0.2748
c --------------------------
c Air p=1.2048x10 -4 g cm-3
c --------------------------
m2 7014 -0.7553 8016 -0.2318 18000 -0.01282 6012 -0.000125
c --------------------------------
c Steel SAE 1020 p=8.0 g cm-3
c --------------------
c m3 6000 -0.002 26000 -0.991
c ---------------------
c Brick, common silica p=1.80 g cm-3
c ------------------------------
c m4 8016 0.663432 13027 0.003747 14000 0.323225 20000 0.007063 26000 0.002534
c ----------------------
c Source Definition
c -------------------
mode n
SDEF PAR=N x=d1 y=d2 z= 500 vec 0 0 -1 dir 1 erg=d3
si1 h -500 500
sp1 d 0 1
si2 h -500 500
sp2 d 0 1
si3 1.00e-9 1.00e-8 1.29e-8 1.66e-8 2.14e-8 2.75e-8 3.55e-8 4.75e-8 5.89e-8 &
   7.59e-8 9.77e-8 1.26e-7 1.62e-7 2.09e-7 2.69e-7 3.47e-7 4.47e-7 &
```

```
    5.75e-7 7.41e-7 9.55e-7 1.23e-6 1.58e-6 2.04e-6 2.63e-6 3.39e-6 &
    4.37e-6 5.62e-6 7.24e-6 9.33e-6 1.20e-5 1.55e-5 2.00e-5 2.57e-5 &
    3.31e-5 4.27e-5 5.50e-5 7.08e-5 9.12e-5 1.17e-4 1.51e-4 1.95e-4 &
    2.51e-4 3.24e-4 4.17e-4 5.37e-4 6.92e-4 8.91e-4 1.15e-3 1.48e-3 &
    1.91e-3 2.45e-3 3.16e-3 4.07e-3 5.25e-3 6.76e-3 8.71e-3 1.12e-2 &
    1.45e-2 1.86e-2 2.40e-2 3.09e-2 3.98e-2 5.13e-2 6.61e-2 8.51e-2 &
    1.10e-1 1.41e-1 1.82e-1 2.34e-1 3.02e-1 3.89e-1 5.01e-1 6.46e-1 &
    8.32e-1 1.07e0 1.38e0 1.78e0 2.29e0 2.95e0 3.80e0 4.90e0 6.31e0 &
    8.13e0 1.05e1 1.35e1 1.74e1 2.24e1 2.88e1 3.72e1 4.79e1 6.17e1 &
    7.94e1 1.02e2 1.32e2 1.70e2 2.19e2 2.82e2 3.63e2 4.68e2 6.03e2 &
    7.76e2 1.00e3
sp3 0 1.26e-3 3.48e-4 8.36e-4 2.05e-3 7.15e-3 5.99e-3 8.95e-3 1.23e-2 &
    2.03e-2 2.13e-2 2.67e-2 2.45e-2 2.77e-2 2.49e-2 1.50e-2 1.53e-2 &
    1.04e-2 8.24e-3 8.47e-4 4.36e-4 2.02e-3 9.15e-4 4.40e-3 3.07e-3 &
    1.53e-3 2.68e-3 4.15e-3 1.23e-3 1.99e-3 1.32e-3 3.09e-3 1.46e-3 &
    1.99e-3 3.15e-3 8.98e-4 1.05e-3 1.74e-3 1.93e-3 2.46e-3 2.41e-3 &
    4.11e-3 5.79e-3 4.48e-3 3.31e-3 3.96e-3 3.49e-3 4.48e-3 1.45e-3 &
    5.52e-3 3.03e-3 3.78e-3 3.89e-3 3.18e-3 2.31e-3 2.60e-3 5.54e-3 &
    1.89e-3 4.32e-3 2.99e-3 1.94e-3 5.09e-3 4.09e-3 1.45e-2 9.03e-3 &
    7.14e-3 8.28e-3 6.06e-3 4.24e-3 8.82e-3 9.25e-3 5.82e-3 1.89e-2 &
    1.61e-2 1.38e-2 1.26e-2 1.17e-2 1.99e-2 2.18e-2 1.36e-2 2.31e-2 &
    1.77e-2 2.08e-2 1.23e-2 5.52e-3 8.68e-3 2.61e-2 1.76e-2 2.32e-2 &
    1.55e-2 2.86e-2 3.55e-2 2.87e-2 3.54e-2 5.00e-2 3.19e-2 2.13e-2 &
    1.43e-2 1.18e-2 5.11e-3 4.89e-3 1.10e-3
c f4:n 2
f14:n 2
fc14 Neutron flux through RPP
FM14 1e6
c e14 1e-8 99log 1e3
nps 10000000
```

APPENDIX H

MCNP6 input file to determine attenuation of cosmic-ray neutrons at 2000 ft

```
c --------NEUTRON BOX ------------------
c -------cell cards--------------------
1 2 -0.00012048 -1 2 3 imp:n=1
2 2 -0.00012048 -2 imp:n=1
3 0 1 imp:n=0
4 4 -1.8 -3 imp:n=1

c -------surface cards----------------------
1 rpp -500 500 -500 500 -500 500
2 rpp -10 10 -10 10 -400 -399
3 rpp -499.9 499.9 -499.9 499.9 -300 -200

c material cards
c ------------------
c Concrete standard p=2.3 g cm-3
c ----------------------
c m1 1001 0.1170 8016 0.6082 14000 0.2748
c --------------------------
c Air p=1.2048x10 -4 g cm-3
c --------------------------
m2 7014 -0.7553 8016 -0.2318 18000 -0.01282 6012 -0.000125
c --------------------------------
c Steel SAE 1020 p=8.0 g cm-3
c --------------------
c m3 6000 -0.002 26000 -0.991
c ---------------------
c Brick, common silica p=1.80 g cm-3
c ------------------------------
m4 8016 0.663432 13027 0.003747 14000 0.323225 20000 0.007063 26000 0.002534
c ----------------------
c Source Definition
c -------------------
mode n
SDEF PAR=N x=d1 y=d2 z= 500 vec 0 0 -1 dir 1 erg=d3
si1 h -500 500
sp1 d 0 1
si2 h -500 500
sp2 d 0 1
si3 1.00e-9 1.00e-8 1.29e-8 1.66e-8 2.14e-8 2.75e-8 3.55e-8 4.75e-8 5.89e-8 &
   7.59e-8 9.77e-8 1.26e-7 1.62e-7 2.09e-7 2.69e-7 3.47e-7 4.47e-7 &
```

5.75e-7 7.41e-7 9.55e-7 1.23e-6 1.58e-6 2.04e-6 2.63e-6 3.39e-6 &
4.37e-6 5.62e-6 7.24e-6 9.33e-6 1.20e-5 1.55e-5 2.00e-5 2.57e-5 &
3.31e-5 4.27e-5 5.50e-5 7.08e-5 9.12e-5 1.17e-4 1.51e-4 1.95e-4 &
2.51e-4 3.24e-4 4.17e-4 5.37e-4 6.92e-4 8.91e-4 1.15e-3 1.48e-3 &
1.91e-3 2.45e-3 3.16e-3 4.07e-3 5.25e-3 6.76e-3 8.71e-3 1.12e-2 &
1.45e-2 1.86e-2 2.40e-2 3.09e-2 3.98e-2 5.13e-2 6.61e-2 8.51e-2 &
1.10e-1 1.41e-1 1.82e-1 2.34e-1 3.02e-1 3.89e-1 5.01e-1 6.46e-1 &
8.32e-1 1.07e0 1.38e0 1.78e0 2.29e0 2.95e0 3.80e0 4.90e0 6.31e0 &
8.13e0 1.05e1 1.35e1 1.74e1 2.24e1 2.88e1 3.72e1 4.79e1 6.17e1 &
7.94e1 1.02e2 1.32e2 1.70e2 2.19e2 2.82e2 3.63e2 4.68e2 6.03e2 &
7.76e2 1.00e3
sp3 0 7.004E-03 3.638E-03 7.733E-03 7.706E-03 1.238E-02 1.573E-02 2.163E-02 &
2.136E-02 2.258E-02 1.706E-02 1.442E-02 9.198E-03 5.150E-03 4.095E-03 &
4.304E-03 3.081E-03 3.719E-03 3.923E-03 3.841E-03 4.291E-03 3.498E-03 &
4.086E-03 3.024E-03 3.052E-03 3.675E-03 3.640E-03 4.842E-03 3.498E-03 &
3.579E-03 3.610E-03 4.949E-03 4.461E-03 5.399E-03 5.821E-03 5.691E-03 &
4.443E-03 3.888E-03 3.998E-03 3.896E-03 4.060E-03 4.196E-03 4.686E-03 &
4.508E-03 3.964E-03 4.825E-03 4.333E-03 4.310E-03 3.581E-03 3.778E-03 &
5.263E-03 4.139E-03 5.496E-03 4.841E-03 6.141E-03 5.105E-03 5.518E-03 &
5.260E-03 5.532E-03 4.669E-03 5.854E-03 5.916E-03 7.793E-03 7.550E-03 &
8.144E-03 8.367E-03 8.543E-03 9.895E-03 1.008E-02 1.246E-02 1.204E-02 &
1.208E-02 1.597E-02 1.925E-02 1.703E-02 2.075E-02 1.913E-02 2.549E-02 &
2.241E-02 1.889E-02 1.987E-02 2.183E-02 1.765E-02 1.492E-02 1.120E-02 &
1.036E-02 1.139E-02 1.237E-02 1.373E-02 1.925E-02 2.165E-02 2.248E-02 &
2.600E-02 3.043E-02 3.046E-02 2.996E-02 1.911E-02 1.369E-02 8.962E-03 &
5.772E-03 3.450E-03 1.712E-03
f14:n 2
fc14 Neutron flux through RPP
FM14 1e6
nps 10000000

APPENDIX I

MCNP6 input file to determine attenuation of cosmic-ray neutrons at 5000 ft

```
c --------NEUTRON BOX ------------------
c -------cell cards--------------------
1 2 -0.00012048 -1 2 3 imp:n=1
2 2 -0.00012048 -2 imp:n=1
3 0 1 imp:n=0
4 3 -8.0 -3 imp:n=1

c -------surface cards----------------------
1 rpp -500 500 -500 500 -500 500
2 rpp -10 10 -10 10 -400 -399
3 rpp -499.9 499.9 -499.9 499.9 -300 -200

c material cards
c ------------------
c Concrete standard p=2.3 g cm-3
c ----------------------
c m1 1001 0.1170 8016 0.6082 14000 0.2748
c --------------------------
c Air p=1.2048x10 -4 g cm-3
c --------------------------
m2 7014 -0.7553 8016 -0.2318 18000 -0.01282 6012 -0.000125
c --------------------------------
c Steel SAE 1020 p=8.0 g cm-3
c --------------------
m3 6000 -0.002 26000 -0.991
c ---------------------
c Brick, common silica p=1.80 g cm-3
c ----------------------------
c m4 8016 0.663432 13027 0.003747 14000 0.323225 20000 0.007063 26000 0.002534
c ----------------------
c Source Definition
c -------------------
mode n
SDEF PAR=N x=d1 y=d2 z= 500 vec 0 0 -1 dir 1 erg=d3
si1 h -500 500
sp1 d 0 1
si2 h -500 500
sp2 d 0 1
si3 1.00e-9 1.00e-8 1.29e-8 1.66e-8 2.14e-8 2.75e-8 3.55e-8 4.75e-8 5.89e-8 &
   7.59e-8 9.77e-8 1.26e-7 1.62e-7 2.09e-7 2.69e-7 3.47e-7 4.47e-7 &
```

5.75e-7 7.41e-7 9.55e-7 1.23e-6 1.58e-6 2.04e-6 2.63e-6 3.39e-6 &
4.37e-6 5.62e-6 7.24e-6 9.33e-6 1.20e-5 1.55e-5 2.00e-5 2.57e-5 &
3.31e-5 4.27e-5 5.50e-5 7.08e-5 9.12e-5 1.17e-4 1.51e-4 1.95e-4 &
2.51e-4 3.24e-4 4.17e-4 5.37e-4 6.92e-4 8.91e-4 1.15e-3 1.48e-3 &
1.91e-3 2.45e-3 3.16e-3 4.07e-3 5.25e-3 6.76e-3 8.71e-3 1.12e-2 &
1.45e-2 1.86e-2 2.40e-2 3.09e-2 3.98e-2 5.13e-2 6.61e-2 8.51e-2 &
1.10e-1 1.41e-1 1.82e-1 2.34e-1 3.02e-1 3.89e-1 5.01e-1 6.46e-1 &
8.32e-1 1.07e0 1.38e0 1.78e0 2.29e0 2.95e0 3.80e0 4.90e0 6.31e0 &
8.13e0 1.05e1 1.35e1 1.74e1 2.24e1 2.88e1 3.72e1 4.79e1 6.17e1 &
7.94e1 1.02e2 1.32e2 1.70e2 2.19e2 2.82e2 3.63e2 4.68e2 6.03e2 &
7.76e2 1.00e3
sp3 0 7.620E-03 4.418E-03 6.468E-03 8.134E-03 1.280E-02 1.382E-02 2.076E-02 &
2.106E-02 2.104E-02 1.782E-02 1.413E-02 8.359E-03 6.096E-03 4.025E-03 &
4.086E-03 3.925E-03 4.178E-03 3.068E-03 3.979E-03 4.244E-03 4.478E-03 &
4.094E-03 4.200E-03 3.926E-03 4.693E-03 4.235E-03 3.965E-03 4.165E-03 &
4.267E-03 4.486E-03 4.516E-03 5.362E-03 4.992E-03 4.026E-03 4.717E-03 &
4.317E-03 4.297E-03 5.024E-03 4.738E-03 4.190E-03 4.658E-03 4.738E-03 &
4.856E-03 5.213E-03 4.681E-03 4.801E-03 4.888E-03 4.635E-03 4.594E-03 &
4.288E-03 4.175E-03 4.948E-03 4.579E-03 5.180E-03 5.247E-03 4.441E-03 &
5.418E-03 4.939E-03 4.988E-03 6.420E-03 6.176E-03 6.435E-03 5.925E-03 &
7.553E-03 8.664E-03 8.476E-03 9.424E-03 1.016E-02 1.194E-02 1.228E-02 &
1.146E-02 1.968E-02 2.137E-02 1.898E-02 2.144E-02 1.983E-02 2.332E-02 &
2.626E-02 1.682E-02 2.125E-02 1.906E-02 1.586E-02 1.409E-02 1.171E-02 &
1.315E-02 1.183E-02 1.309E-02 1.414E-02 1.778E-02 1.874E-02 2.438E-02 &
2.704E-02 2.945E-02 2.720E-02 2.463E-02 1.877E-02 1.394E-02 9.170E-03 &
6.709E-03 3.563E-03 1.835E-03
f14:n 2
fc14 Neutron flux through RPP
FM14 1e6
nps 10000000